`GarajHubbardGolovchenko2010`

Graphene synthesis by ion implantation

Slaven Garaj,[1] William Hubbard,[2] and J. A. Golovchenko[1,2,a]

[1]*Department of Physics, Harvard University, 17 Oxford Street, Cambridge, Massachusetts 02138, USA*
[2]*School of Engineering and Applied Sciences, Harvard University, 29 Oxford Street, Cambridge, Massachusetts 02138, USA*

We demonstrate an ion implantation method for large-scale synthesis of high quality graphene films with controllable thickness. Thermally annealing polycrystalline nickel substrates that have been ion implanted with carbon atoms results in the surface growth of graphene films whose average thickness is controlled by implantation dose. The graphene film quality, as probed with Raman and electrical measurements, is comparable to previously reported synthesis methods. The implantation synthesis method can be generalized to a variety of metallic substrates and growth temperatures, since it does not require a decomposition of chemical precursors or a solvation of carbon into the substrate. © *2010 American Institute of Physics*. [doi:10.1063/1.3507287]

Graphene, with its unique physical and structural properties, has recently become a proving ground for various physical phenomena,[1–3] and it is a serious candidate for a variety of electronic and energy-related device applications.[4–6] The physical properties of graphene depend sensitively on its thickness. For example, bilayer graphene exhibits a tunable electronic bandgap,[7,8] whereas monolayer graphene is gapless. A major challenge in achieving the practical potential of graphene is rational synthesis of large-scale graphene films with tunable thickness, compatible with established large-scale semiconductor technologies. Recently, scalable graphene growth methods, based on *dissolution-precipitation*[9–12] and *surface adsorption*[13] synthesis methods, have been reported. In the first case, nickel substrates heated at ∼1000 °C dissolve carbon, usually generated from chemical vapor deposition (CVD) of hydrocarbons.[9–11] As the Ni film is subsequently cooled, the bulk carbon solubility is reduced and carbon segregates on the Ni surface and crystallizes into graphene. Thickness control remains challenging; only a fraction of available source carbon precipitates into graphene, with an efficiency that depends critically on process parameters. On the other hand, CVD surface adsorption on a copper substrate[13] is a self-limiting process that produces only single-layer graphene.

In this letter, we report an *ion implantation* method for graphene synthesis with potential layer-by-layer thickness control. The method uses ion-implantation to introduce a precise dose of carbon atoms into polycrystalline nickel films, and subsequent graphene growth on Ni film surface upon heat treatment. The carbon doses we use in this work correspond to 15% or less of the saturated carbon concentration in nickel during the CVD process[14] at 1000 °C. Since almost all of the implanted carbon atoms crystallize into graphene, the method potentially offers more graduated control of graphene thickness than is achievable by the CVD-on-Ni process. The ion-implantation method does not require the metal film to have high carbon solubility (unlike the dissolution-precipitation process), so it can be generalized to other substrates. As an additional advantage, ion implanta-

tion is a mature technology commonly used in the electronic industry, and it takes the graphene synthesis into the realm of large-scale semiconductor foundries.

In the first step of the process, we evaporated 500 nm of Ni onto Si/SiO₂ wafers. These were then annealed in Ar and H₂ flow at 1000 °C at ambient pressure for 2 h, leading to recrystallization of the Ni film into grains of ∼2 μm average size (log-normal grain size distribution with mean μ =1.6 μm and standard deviation σ=0.35, as determined by optical microscopy). X-ray diffraction analysis of the annealed thin film revealed only Ni(111) oriented parallel to the film thickness as expected.[15] The Ni films were implanted with 30 keV carbon ions at *Varian Semiconductor Equipment Associates* and at *Core Systems*, with doses of 2 $\times 10^{15}$, 4×10^{15}, 7.9×10^{15}, and 1.3×10^{16} ions/cm², which correspond approximately to the surface atomic thicknesses of carbon contained in 0.5, 1, 2, and 3 graphene monolayers (ML), respectively. The average carbon ion penetration depth is ∼40 nm and the implantation dose is uniform in area density and accurate to ∼1%. The shallow ion implantation at the above doses does not perturb crystalline grain structure of a metallic substrate.[16] The implanted sample was mounted on a button heater in a vacuum chamber (5×10^{-8} Torr) and heated rapidly to 1000 °C, leading to diffusion of the carbon atoms within the Ni film. After dwelling at 1000 °C for ∼1 h, the samples were slowly cooled to room temperature at rates of 5–20 °C/min. As the solubility of carbon in the film decreased with decreasing temperature, the carbon atoms formed graphene at the surface. Comparison of x-ray diffraction spectra and optical images from the Ni film before and after the graphene growth reveals no change in orientation or sizes of Ni grains.

Figure 1(a) shows an optical image of a graphene film grown from a polycrystalline Ni film implanted with 7.9 $\times 10^{15}$ C atoms/cm² (2 ML dose) and transferred to a Si/SiO₂ chip using the standard PMMA transfer method.[10] Raman spectroscopy [Fig. 1(b)] reveals spectral features, uniquely characteristic of graphene films;[17,18] a G (1590 cm⁻¹) peak associated with sp^2 carbon bond stretching, a G′ (2700 cm⁻¹) peak sensitive to graphene inter layer interactions, and a D (1350 cm⁻¹) peak arising from symmetry-breaking features, such as graphene defects and

a)Author to whom correspondence should be addressed. Electronic mail: golovchenko@physics.harvard.edu. Tel.: 617-495-3905. FAX: 617-496-0189.
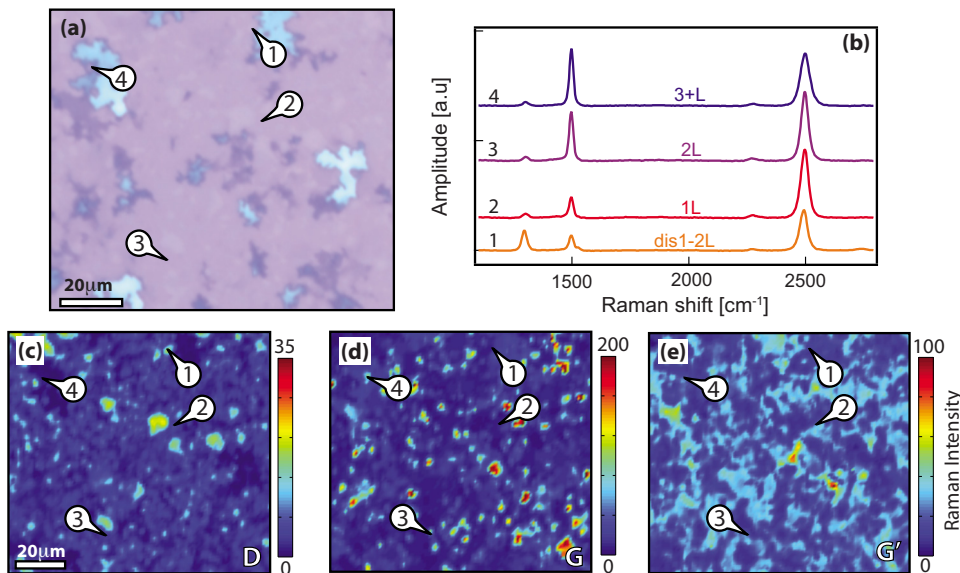
FIG. 1. (Color online) (a) Optical image of graphene film grown on nickel implanted with 7.9×10^{15} C atoms/cm^2 (2 ML), and subsequently transferred to Si/SiO$_2$ substrate. (b) Characteristic Raman spectra taken at the marked positions in the optical image, revealing regions of high-quality monolayer and bilayer graphene (1L, 2L), thicker regions (3 +L), and thin, disordered graphene (dis1–2L). [(c)–(e)] Spatial maps of D, G, and G′ Raman peak intensities, respectively, in the same field of view as the optical image.

domain boundaries. To gain insight into the spatial homogeneity of the grown film, Raman spectral spatial maps were taken at 1 μm steps across the same 100×90 μm^2 area that covers the optical image in Fig. 1(a). At each location, Raman peaks were fitted with Lorentzian functions. Intensity maps for D, G, and G′ peaks are presented in Figs. 1(c)–1(e). The overall low intensity of the disorder-defined D peak indicates that all but isolated patches of the graphene film are of high quality. The relative ratio of G/G′ peaks— determined by the number of stacked graphene layers— confirms the film is mostly (~75%) one to two layer thick (denoted 1–2L) low-defect graphene. The rest of the film is comprised of ~20% graphene that is more than three layers thick (3+L), and of isolated regions (~5%) of moderately disordered one to two layer graphene (dis1–2L).

The structure of the graphene film appears to reflect the polycrystalline map of the underlying Ni substrate. The thicker 3+L regions follow the veins of the grain boundaries, as similarly observed in CVD grown films.[10] The rest of the film consists of micron-sized graphene domains of different thickness, even though the source carbon was implanted uniformly and shallowly in the Ni substrate. We conclude that the implanted carbon atoms at ~1000 °C are highly mobile and are transported over a range spanning at least ~10 μm, enabling a heterogeneous graphene thickness distribution on the surface of the Ni film. Furthermore, the dynamics of graphene growth varies between different nickel grains, leading to varying degrees of disorder and thickness in corresponding graphene domains. We presume that the graphene growth is driven by the surface properties and morphology of the Ni grains.[19]

Raman spectral analysis of samples prepared with increasing implant doses—carbon surface densities equivalent to 0.5, 1, 2, and 3 ML of graphene—reveals an increase in the overall film quality and thickness with increasing dose. A single Raman spectrum cannot properly characterize a large-scale graphene film with inhomogeneous domains. So we acquired, for each implantation dose, Raman maps from two separate 100×90 μm^2 regions with 1×1 μm^2 sampling. The Raman intensity ratios of the D to G peaks (measure of disorder), and G to G′ peaks (measure of thickness), are calculated for each sampled region and plotted (Fig. 2). The

color scale corresponds to the number of sample segments within Raman ratio bins of 0.05×0.05. For implantation doses of 1 ML, 2 ML, and 3 ML, the majority of the corresponding film (~75%) is comprised of low-defect graphene whose average thickness monotonically increases from one to two layers for the 1 ML dose, to two to three layers for the 3 ML dose. This is indicated in Fig. 2 as a shift in the densities toward larger G/G′ values[18] with increased dose, and in Fig. 3(a) as a dose dependence of the averaged $\langle G/G' \rangle$.

A close inspection of the density plots in Fig. 2 reveals that the 0.5 ML film largely consists of defected one to two layer graphene (dis1–2L), likely in the form of percolative
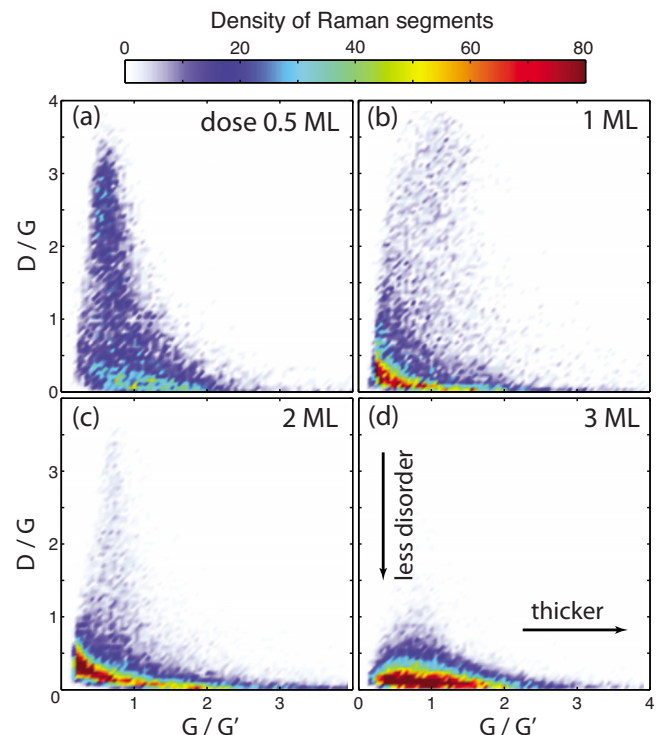

FIG. 2. (Color online) Plots showing Raman D/G and G/G′ peak intensity ratios, respectively, for (a) 0.5 ML, (b) 1 ML, (c) 2 ML, and (d) 3 ML implantation doses. The color scale indicates the number of 1×1 μm^2 segments in Raman maps that correspond to given D/G and G/G′ intensity ratios within the bin size of 0.05×0.05.
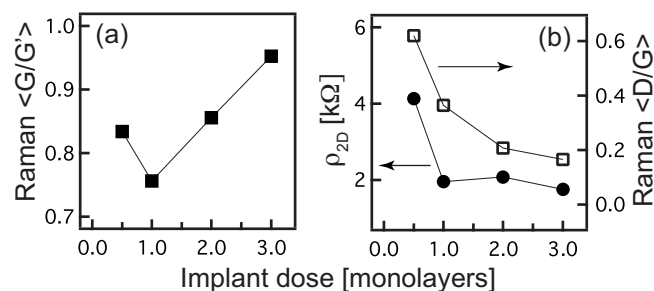
FIG. 3. (a) Average $\langle G/G' \rangle$ Raman ratio versus implantation dose showing an increased graphene thickness with implantation dose. (b) 2D resistivity of graphene films (full circles) and averaged $\langle D/G \rangle$ Raman ratio (open squares) correlate decrease in resistivity and disorder with increased implantation dose.

networks. The disorder progressively decreases for the 1 ML and 2 ML doses, and is strongly suppressed for the 3 ML dose, as observed in the shift in the distributions toward low D/G values [Figs. 2(b)–2(d)]. We conclude that the disorder is primarily driven by the deficiency of source carbon atoms, coupled with the difference in graphene growth affinities at different Ni grains. The regions of remnant disorder in 3 ML film are localized to the edges of graphene domain boundaries (Raman spatial maps not shown), indicating that the secondary source of defects stems from imperfect matching of the graphene domains.

The thicker 3+L regions of the graphene cover $\sim 15\% - 20\%$ of the surface for all implantation doses, indicating that the corresponding Ni surface sites near the crystallite boundaries are energetically favorable for carbon segregation, even in the case of overall carbon-deficiency. A coarse comparison of the average graphene thickness versus implantation dose indicates that most of the implanted carbon atoms are incorporated into the grown graphene.

The electrical properties of the graphene films transferred to the Si/SiO_2 wafers were obtained by patterning $5-10$ μm wide strips using optical lithography and oxygen-plasma etching. The graphene strips were contacted by evaporated Cr/Au electrodes separated by $10-15$ μm and their resistance was measured at room temperature. Figure 3(b) depicts two-dimensional (2D) resistivity and averaged $\langle D/G \rangle$ Raman ratio of graphene films as a function of the implantation dose, demonstrating the expected correlation between resistivity and disorder in those films. For the 0.5 ML film, the graphene strips in many of the corresponding electronic devices, presumably with higher defect content, did not withstand the fabrication process. Hence, the measured mean resistivity ρ_{2D} (0.5 ML)=4 $k\Omega/sq$ is only a lower limit. For 1 ML, 2 ML, and 3 ML films, the resistivities are dose-independent at $\rho_{2D} \approx 2$ $k\Omega/sq$. This is in line with the resistivities previously reported for CVD-grown graphene films[10,20] and exfoliated graphene multilayers,[21] and confirms the overall good electrical quality of the films.

In conclusion, we have demonstrated a method for the synthesis of graphene films of tunable thickness using ion implantation to introduce a precise amount of source carbon into the Ni substrate. We observe implantation dose dependence in various film properties; increased dose leads to gradual increase in average graphene thickness and decrease in its defect content. Distinctive advantages of the ion implantation method over the others—such as CVD—are that it can be generalized to other metallic substrates regardless of their carbon solubility, and it is not limited to the growth temperatures needed to decompose precursor molecules. The ability to prepare large homogeneous films with a precisely controlled number of layers requires further optimization of substrate surface homogeneity. Surface diffusion of carbon atoms to, and on, inhomogeneous surfaces limits the large-length scale homogeneity of fabricated material. Its control through materials choice, optimized thermal processing, and diffusion barriers may remedy this problem.

[1] A. K. Geim and K. S. Novoselov, Nature Mater. **6**, 183 (2007).
[2] A. K. Geim, Science **324**, 1530 (2009).
[3] A. H. C. Neto, N. M. R. Peres, K. S. Novoselov, and A. K. Geim, Rev. Mod. Phys. **81**, 109 (2009).
[4] X. Wang, L. Zhi, and K. Mullen, Nano Lett. **8**, 323 (2008).
[5] M. D. Stoller, S. Park, Y. Zhu, J. An, and R. S. Ruoff, Nano Lett. **8**, 3498 (2008).
[6] Y.-M. Lin, K. A. Jenkins, A. Valdes-Garcia, J. P. Small, D. B. Farmer, and P. Avouris, Nano Lett. **9**, 422 (2009).
[7] K. Eduardo, C. Novoselov, S Morozov, N Peres, J. D. Santos, J. Nilsson, F. Guinea, A. Geim, and A. Neto, Phys. Rev. Lett. **99**, 216802 (2007).
[8] J. B. Oostinga, H. B. Heersche, X. Liu, A. F. Morpurgo, and L. M. K. Vandersypen, Nature Mater. **7**, 151 (2007).
[9] Y. Qingkai, J. Lian, S. Siriponglert, H. Li, Y. P. Chen, and S.-S. Pei, Appl. Phys. Lett. **93**, 113103 (2008).
[10] A. Reina, X. Jia, J. Ho, D. Nezich, H. Son, V. Bulovic, M. S. Dresselhaus, and J. Kong, Nano Lett. **9**, 30 (2009).
[11] K. S. Kim, Y. Zhao, H. Jang, S. Y. Lee, J. M. Kim, K. S. Kim, J.-H. Ahn, P. Kim, J.-Y. Choi, and B. H. Hong, Nature (London) **457**, 706 (2009).
[12] M. Zheng, K. Takei, B. Hsia, H. Fang, X. Zhang, N. Ferralis, H. Ko, Y.-L. Chueh, Y. Zhang, R. Maboudian, and A. Javey, Appl. Phys. Lett. **96**, 063110 (2010).
[13] X. Li, W. Cai, J. An, S. Kim, J. Nah, D. Yang, R. Piner, A. Velamakanni, I. Jung, E. Tutuc, S. Banerjee, L. Colombo, and R. Ruoff, Science **324**, 1312 (2009).
[14] W. W. Dunn, Rice University, 1970.
[15] S. Thiele, A. Reina, P. Healey, J. Kedzierski, P. Wyatt, P.-L. Hsu, C. Keast, J. Schaefer, and J. Kong, Nanotechnology **21**, 015601 (2010).
[16] G. Dearnaley, Annu. Rev. Mater. Sci. **4**, 93 (1974).
[17] A. C. Ferrari, J. C. Meyer, V. Scardaci, C. Casiraghi, M. Lazzeri, F. Mauri, S. Piscanec, D. Jiang, K. S. Novoselov, S. Roth, and A. K. Geim, Phys. Rev. Lett. **97**, 187401 (2006).
[18] L. M. Malard, M. A. Pimenta, G. Dresselhaus, and M. S. Dresselhaus, Phys. Rep. **473**, 51 (2009).
[19] J. C. Shelton, H. R. Patil, and J. M. Blakey, Surf. Sci. **43**, 493 (1974).
[20] M. P. Levendorf, C. S. Ruiz-Vargas, S. Garg, and J. Park, Nano Lett. **9**, 4479 (2009).
[21] K. Nagashio, T. Nishimura, K. Kita, and A. Toriumi, Jpn. J. Appl. Phys., Part 1 **49**, 051304 (2010).